© IIJP 2025 | Volume 1, Issue 4, pp. 82-105 | ISSN: 2636-4484

A NUMERICAL STUDY OF HEAT AND MASS TRANSFER IN A VERTICAL CHANNEL DUE TO INFLUENCE OF TEMPERATURE-DEPENDENT VISCOSITY, THERMAL RADIATION AND SUCTION/INJECTION

Yusuf A.B,[1], Bello Y.[2] & Umar A.[3]

Department of Mathematics, Federal University Dutsin-ma, Katsina States, Nigeria.
Corresponding author: aliyuumar2029@gmail.com

ARTICLE INFO

Article No.: 073

Accepted Date: 07/10/2025

Published Date: 21/10/2025

Type: Research

ABSTRACT

This study presents a numerical investigation of heat and mass transfer in a vertical channel considering the combined effects of temperature-dependent viscosity, thermal radiation, and suction. The objective is to understand how these factors influence velocity, temperature, and concentration distributions, which are critical in heat and mass transfer applications. The governing nonlinear differential equations were formulated, non-dimensionalized, and solved using the finite difference method, with MATLAB employed for coding and simulation. Results are reported through graphical and tabular analyses. The findings reveal that fluid velocity decreases with a reduction in the Grashof number, whereas higher Prandtl numbers enhance both velocity and temperature. An increase in the radiation parameter broadens the velocity field, while greater Schmidt numbers reduce both velocity and concentration. Overall, the results provide new insight into the interplay of variable viscosity, radiation, and suction in convective transport, offering practical relevance for engineering systems involving heat exchangers, porous media flows, and radiative environments.

Keywords: Vertical channel flow, temperature-dependent viscosity, thermal radiation, suction, finite difference method, convective heat and mass transfer.

1.0 INTRODUCTION

Free convection in vertical channels plays a vital role in heat exchangers, electronic cooling, nuclear systems, and solar collectors. Such flows are governed by buoyancy effects but are further modified by factors such as variable viscosity, thermal radiation, and wall suction. Viscosity variations strongly influence velocity and shear stress, while radiation dominates in high-temperature environments by altering temperature and velocity distributions. Suction helps stabilize boundary layers and affects transfer rates.

Although these effects have been studied individually, limited work addresses their combined influence in vertical channel flows. This study fills that gap by numerically investigating mass transfer with temperature-dependent viscosity, thermal radiation, and suction using the finite difference method in MATLAB.

Free convection in a boundary layer arises primarily from the interplay between gravitational forces and density variations induced by temperature or concentration gradients. Theoretical models of convection in parallel-plate or vertical-plate channels typically assume constant surface temperature, ramped wall temperature, or uniform heat flux. More recent investigations have extended these classical assumptions to include magnetic fields, Hall currents, radiation, porous structures, variable viscosity, and transient effects, thereby capturing more realistic physical scenarios (Mahdy & Chamkha, 2019; Roy et al., 2021).

The role of thermal radiation in convective heat transfer is particularly important in high-temperature environments. Studies have shown that radiation modifies both velocity and temperature fields, reduces boundary layer thickness, and elevates wall surface temperatures (Raptis & Perdikis, 2006; Das et al., 2020). Numerical simulations in porous channels reveal that higher values of the radiation parameter generally thin the velocity and thermal layers, whereas increased wall temperature ratios lead to thickening, with suction serving to stabilize the boundary layer (Zaheer & Tasawar, 2007; Ferdousi et al., 2013). More recent contributions confirm that radiation effects are especially significant when coupled with Soret and Dufour diffusion processes (Alharbi et al., 2014).

The influence of variable fluid properties has also been a key focus. Investigations into variable viscosity and internal heat generation demonstrate that viscosity strongly impacts surface shear stress, heat transfer rates, and overall flow stability (Makinde & Ogulu, 2008; Ferdousi et al., 2013). When combined with magnetic fields and radiation, viscosity variation leads to complex couplings that affect both heat and mass transfer. Studies of convection in porous media modeled by Darcy–Brinkman–Forchheimer formulations also show that permeability, Darcy number, and porosity play dominant roles in modifying Nusselt and Sherwood numbers (Elgazery, 2011; Li et al., 2020).

Another important factor in porous media convection is viscous (Darcy) dissipation, whose inclusion in the energy equation has been shown to significantly alter temperature fields. Neglecting this term can lead to substantial underestimation of heat transfer rates, particularly in mixed convection systems (Mahdy & Chamkha, 2019). Recent computational analyses incorporating dissipation effects confirm its role in enhancing energy transport under combined buoyancy and radiative conditions (Ahmed et al., 2021).

Unsteady free convection flows have also been widely studied due to their relevance in industrial processes such as cooling of nuclear systems, material processing, and electronic devices. Transient models show that velocity and temperature profiles evolve significantly from initial conditions before reaching steady state (Hossain & Wilson, 2003; Roy et al., 2021). Recent developments using finite element, Keller-Box, and lattice Boltzmann methods have further demonstrated the influence of wall roughness, channel curvature, and microstructure geometry on unsteady convection dynamics (Li et al., 2020; Wang et al., 2022).

Research on heat and mass transfer in vertical channels continues to expand toward application-driven problems. For instance, numerical studies of shear flow over herringbone microstructures have revealed that microstructure-induced oscillations and recirculation enhance transfer rates, with scaling laws linked to Reynolds and Schmidt numbers (Wang et al., 2022). Investigations into helium-chilled copper tubes under sudden vacuum loss have provided practical correlations for predicting freeze range and mitigating frost contamination in cryogenic accelerators (Bao et al., 2023). Similarly, recent work on rapid mass transfer in binary systems has introduced unified models for accurately predicting mass loss rates in astrophysical and engineering contexts (Ivanova et al., 2024).

Finally, advances in computational fluid dynamics (CFD) have been central to progress in this field. Classical approaches such as the SIMPLE algorithm and finite element methods remain widely used, but recent work has refined numerical schemes to improve efficiency and stability for highly nonlinear radiation–convection problems (Kumar & Singh, 2022). These advances provide more accurate simulation platforms for addressing the interplay of thermal radiation, variable properties, porous media, and transient free convection in vertical channels.

2.0 MATHEMATICAL PROBLEM

The physical problem under consideration consists of a vertical channel formed by two infinite parallel plates kept h distance apart with the channel filled with an optically thick incompressible viscous fluid in the presence of an incidence radiative heat flux of intensity q_r which is absorbed by the plates and transferred to the fluid as shown in figure 1 below. The fluid properties are all assumed to be constant except for its viscosity which is temperature-dependent. Since the fluid is optically thick, the radiative heat flux in the flow formation is expanded using non-linear Rosseland heat diffusion. At time t, both the fluid and the plates are assumed to be at rest with constant temperature T_0. At time $t > 0$, the temperature of the plate kept at $y' = 0$ rise to T_w while the other plate at $y' = h$ is fixed and maintained at temperature T_0. The stream wise coordinate is denoted by x'- axis taken along the channel in the vertically upward direction and that normal to it is denoted by y'. Fully developed flow is considered in this model meaning that the axial (x'-direction) velocity depends only on the transverse co-ordinate y'. Furthermore; in the flow, the effect of viscous dissipation is taken into account while that of the radiative heat flux in the x' direction is assumed to be negligible compared to that in the y'- direction. Since the plates are of infinite length, the velocity and temperature are functions of y and t only.

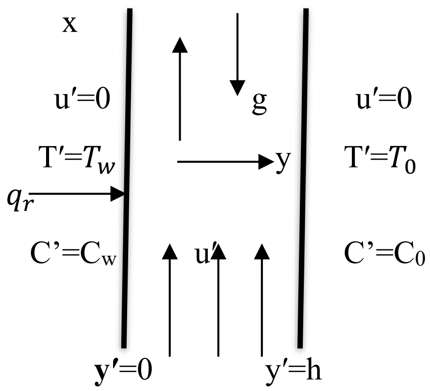

Figure 1: schematic diagram

Under these assumptions, the appropriate governing equations for the present problem in dimensional form are:

$$\frac{\partial u'}{\partial t}+V_0\frac{\partial u'}{\partial y'}=\frac{1}{\rho}\frac{\partial}{\partial y'}\left(\mu\frac{\partial u'}{\partial y'}\right)+g\beta r(T'-T_0)+g\beta c(C'-C_0) \quad 1$$

$$\frac{\partial T'}{\partial t}+V_0\frac{\partial T}{\partial y'}=\alpha\left(\frac{\partial^2 T}{\partial y^2}-\frac{1}{k}\frac{\partial qr}{\partial y'}\right)+\frac{\mu}{\rho Cp}\left(\frac{\partial u'}{\partial y'}\right)^2+\frac{Q_0}{\rho Cp}(T'-T_0) \quad 2$$

$$\frac{\partial C'}{\partial t}+V_0\frac{\partial C'}{\partial y'}=D\frac{\partial^2 C'}{\partial y^2} \quad 3$$

The boundary conditions are:

$$\left.\begin{array}{ll} u' = 0, C' = C_W\ T' = T_\omega & at\ y' = 0, \\ u' = 0, C' = C_0\ , T' = T_0 & at\ y' = h \end{array}\right\} \quad (4)$$

The fluid dynamic viscosity (μ) is assumed to vary with temperature difference given as:

$$\mu = \mu_0(1-\lambda\theta(y)), \qquad \lambda\epsilon R \quad (5)$$

And the radiative heat flux q_r as given by Sparrow and Cess (1962) is:

$$q_r = \frac{-4\sigma\partial T^4}{3\delta\partial y} \quad (6)$$

3.0 Non-dimensionalisation of the equations.

The following quantities below are suitable to transform the models into dimensionless form:

$$\left.\begin{array}{l}\mu = \mu_0\left(1-\lambda\left(\frac{T'-T_0}{T_\omega - T_0}\right)\right),\quad u = U_0 f(y),\quad y = \frac{y'}{\sqrt{vt}},\quad \theta(y) = \frac{T'-T_0}{T_\omega - T_0}, \\ \delta = 2\sqrt{vt} \qquad \phi(y) = \frac{C'-C_0}{C_w - C_0}\end{array}\right\} \tag{7}$$

Using equation (7) in equation (1), the momentum equation is transform into:

$$\begin{aligned} f''(y) &= \left(\frac{-1}{2}\right)(y+c)\bullet f'(y)(1+\lambda\bullet\theta(y))(1-\lambda\bullet\theta(y))+\lambda\bullet\theta'(y)f'(y)(1+\lambda\theta(y) \\ &-Gr\bullet\theta(y)(1+\lambda\bullet\theta(y))(1-\lambda\bullet\theta(y))-Gc\bullet\phi(y)\bullet(1+\lambda\bullet\theta(y))(1-\lambda\bullet\theta(y)) \end{aligned} \tag{8}$$

$$Gr = \frac{g\beta r(T_w - T_0)\delta^2}{4U_0\vartheta}, Gc = \frac{g\beta c(C_w - C_0)\delta}{4U_0\vartheta}$$

Similarly, using equation (6) and (7) in equation (2), the energy equation is transform into:

$$-\frac{1}{2}(y+C)\theta'(y)(T_w - T_0) = \frac{1}{P_r}\left[\theta''(y)(T_W - T_0) + \frac{4\sigma}{3k\delta}\frac{\partial^2 T^4}{\partial y'^2}\right] + \frac{U_0^2}{\vartheta\rho C_p}(f'(y))^2$$

(9)

But $\frac{\partial^2 T^4}{\partial y^2} = \frac{\partial^2}{\partial y^2}[\theta(y)(T_W - T_0)]^4 = \frac{\partial}{\partial y}[4(\theta(y)(T_w - T_0) + T_0)^3 \cdot \theta'(y)(T_w - T_0)]$

$$\frac{\partial^2 T^4}{\partial y^2} = 4\cdot 3(\theta(y)(T_W - T_0) + T_0)^4 \cdot \theta'(y)(T_W - T_0)\cdot\theta'(y)(T_W - T_0) + 4(\theta(y)(T_W - T_0) + T_0)^3 \cdot \qquad \theta''(y)(T_W - T_0)$$

$$\frac{\partial^2 T^4}{\partial y^2} = 4\cdot 3(T_w - T_0)^2\left[\theta(y) + \frac{T_0}{T_w - T_0}\right]^2 \cdot \theta'(y)^2(T_w - T_0)^2 + 4(T_w - T_0)^3\left[\theta(y) + \frac{T_0}{T_w - T_0}\right]^3 \cdot \theta''(y)(T_w - T_0)$$

$$\frac{\partial^2 T^4}{\partial y^2} = \qquad 4\cdot 3(T_w - T_0)^4[\theta(y) + \phi]^2\theta'(y)^2 + 4(T_w - T_0)^4[\theta(y) + \phi]^3 \cdot \theta''(y)$$

(10)

Now substituting equation (10) into equation (9) we get;

$$\theta''(y) = \left(\frac{-1}{2}\right) \bullet \Pr(y+c) \bullet \theta'(y)\left(1 - \frac{4R}{3}(\theta(y)+\phi)^3\right)$$
$$-4 \bullet R(\theta(y)+\phi))^2(\theta'(y))^2\left(1 - \frac{4R}{3}(\theta(y)+\phi)^3\right)$$
$$-Br(1-\lambda \bullet \theta(y))(1+\lambda \bullet \theta(y))(f'(y))^2\left(1 - \frac{4R}{3}(\theta(y)+\phi)^3\right)$$
$$-Q\theta(y)\left(1 - \frac{4R}{3}(\theta(y)+\phi)^3\right) \tag{11}$$

Similarly, from equation (7) into equation (3) we have;

$$\frac{-1}{2}(y+c)\phi'(y) = \frac{1}{Sc}\phi''(y) \tag{12}$$

Again, using equation (4) the boundary conditions will be transformed into:

$$u = U_0, \quad T = T_W \quad at \quad y = 0$$

$\Longrightarrow f(0) = 0,\ \theta(0) = 0$ at y = 0. $at\ y = h\ (the\ length\ of\ the\ channel)\ \theta(y) = f(y) = 1.$
(13)

Where $Gr = \frac{g\beta(T_W - T_0)\delta^2}{4\vartheta U_0}$, $Ec = \frac{{U_0}^2}{C_p(T_W - T_0)}$, $C = -\frac{vt^{\frac{1}{2}}}{\sqrt{\vartheta}}$, $R = \frac{4\sigma(T_W - T_0)^3}{3K\delta}$, $\phi = \frac{T_W}{T_W - T_0}$, $P_r = \frac{\vartheta}{\alpha}$

$$Sc = \frac{\vartheta}{D}, Gc = \frac{g\beta(C_w - C_0)\delta^2}{4\vartheta U_0},$$
$$Pr * Ec = Br \tag{14}$$

4.0 Method of solution

4.1 Mathematical Description of FDM

The Finite Difference Method (FDM) is a numerical technique used to solve differential equations by approximating derivatives with finite differences. This method involves discretizing the continuous domain (spatial or temporal) into a finite set of points and then approximating the derivatives at these points using difference equations. The following steps are important in solving ODE's using finite difference method;

i. Discretization: The continuous domain is divided into a grid of discrete points. For example, if we have a domain [a, b], we can divide it into (N) intervals of equal length (h = {b-a}/N).

ii. Finite Difference Approximation: Derivatives in the differential equation are replaced with finite difference approximations. For instance, the first derivative of a function (u(x)) at a point (x_i) can be approximated using Central Difference Method:

$$\frac{du}{dx} \approx \frac{u_{i+1}-u_{i-1}}{2h} \qquad (15)$$

$$\frac{d^2u}{dx^2} \approx \frac{u_{i-1}-2u_i+u_{i+1}}{h^2} \qquad (16)$$

4.2 Finite difference method (FDM) Solution of the Problem

Equation (8), (11) and (12) under the boundary conditions (13) are solved using FDM as follows:

$$\frac{f_{i-1}-2f_i+f_{i+1}}{h^2} = \frac{-1}{2}(y_i+c)\left(\frac{f_{i+1}-f_{i-1}}{2h}\right)(1+\lambda\theta(y))(1-\lambda\theta(y))$$
$$+\lambda\left(\frac{\theta_{i+1}-\theta_{i-1}}{2h}\right)\left(\frac{f_{i+1}-f_{i-1}}{2h}\right)(1+\lambda\theta(y))-Gr\theta(y)(1+\lambda\theta(y))(1-\lambda\theta(y))$$
$$-Gc\phi(y)(1+\lambda\theta(y))(1-\lambda\theta(y)) \qquad (17)$$

$$\left(\frac{\theta_{i-1}-2\theta_i+\theta_{i+1}}{h^2}\right) = \frac{-1}{2}\Pr(y_i+c)\left(\frac{\theta_{i+1}-\theta_{i-1}}{2h}\right)\left(1-\frac{4R}{3}(\theta(y)+\phi)^3\right)$$
$$-4R(\theta(y)+\phi)^2\left(\frac{\theta_{i+1}-\theta_{i-1}}{2h}\right)^2\left(1-\frac{4R}{3}(\theta(y)+\phi)^3\right)$$
$$-Br(1-\lambda\theta(y))(1+\lambda\theta(y))\left(\frac{f_{i+1}-f_{i-1}}{2h}\right)^2\left(1-\frac{4R}{3}(\theta(y)+\phi)^3\right)-Q\theta(y)\left(1-\frac{4R}{3}(\theta(y)+\phi)^3\right) \qquad (18)$$

$$\frac{-1}{2}(y_i+c)\left(\frac{\phi_{i+1}-\phi_{i-1}}{2h}\right) = \frac{1}{Sc}\left(\frac{\phi_{i-1}-2\phi_i+\phi_{i+1}}{h^2}\right) \qquad (19)$$

4.3 Nusselt Number, Skin Friction and Sherwood on the Channel Plates.

Since the fluid viscosity considered in this work has variable status, the skin friction on the plates is evaluated following Yusuf *et al* (2020):

$\tau_0 = (1-\lambda\theta)\frac{df}{dy}$ $at\ y = 0$ and $\tau_1 = (1-\lambda\theta)\frac{df}{dy}$ at $y = 1$. (20)

While the Nusselt Number is calculated via:

$Nu_0 = -\frac{d\theta}{dy}$ $at\ y = 0$ and $Nu_1 = -\frac{d\theta}{dy}$ $at\ y = 1$ (21)

To find the Sherwood number on the channel walls we employ the following formula at y = 0 and y = 1 respectively, $Sh_0 = \frac{d\phi}{dy}$ $and\ Sh_1 = \frac{d\phi}{dy}$.

(22)

5.0 RESULTS AND DISCUSSION

Using computer algebra software package (Matlab), equations (10) and (11) are simulated and the results are presented in figure 2-9 and in table I and II. The ambient Prandtl number is taken as 0.71 and which correspond to air and R-12 refrigerant respectively. The number of subintervals N is chosen as 100 and the step size h is 0.01 on the interval [1,0] where a = 1 and b = 0. Similarly, the values of radiation, suction and viscosity variation parameters are chosen arbitrarily from 0 to 3. In addition, the value of Grashof number is taken to be 10, 12, 14. That is, Gr > 0 which also corresponds to cooling of the channel by free convection current.

5.1 Graphical Results

This section presents the numerical results obtained from the finite difference solution of the governing equations. The velocity, temperature, and concentration profiles are displayed graphically to illustrate the influence of key dimensionless parameters, including the Grashof number (Gr), Prandtl number (Pr), radiation parameter (R), and Schmidt number (Sc). The results are compared under different parameter variations to highlight their impact on flow behavior and transport characteristics.

In particular, the discussion focuses on how buoyancy (Gr) modifies velocity, how fluid properties (Pr) affect both momentum and energy transport, how radiation (R) alters the thermal boundary layer, and how mass diffusivity (Sc) influences concentration fields. Tables of skin friction, Nusselt number, and Sherwood number are also included to provide quantitative insight into surface transport phenomena. Together, the graphical and tabular results offer a comprehensive understanding of the coupled effects of viscosity variation, radiation, and suction in vertical channel flows.

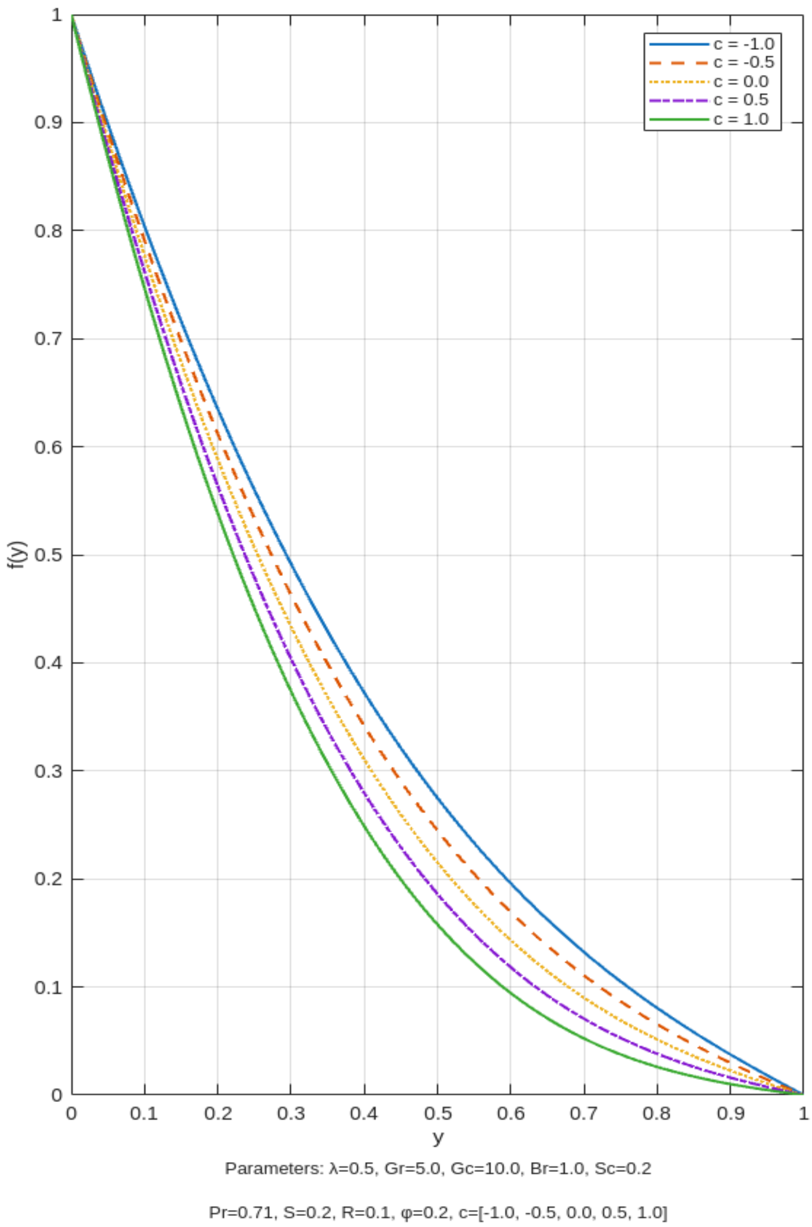

Figure 4.2 Velocity Profile for Various Values of Suction Parameter (C)

Figure 4.2 shows that as suction parameter C increases, the velocity profile decreases, indicating that suction reduces the flow speed by extracting fluid from the boundary layer. Lower values of C (blowing or injection) enhance the velocity since fluid is pushed into the domain.

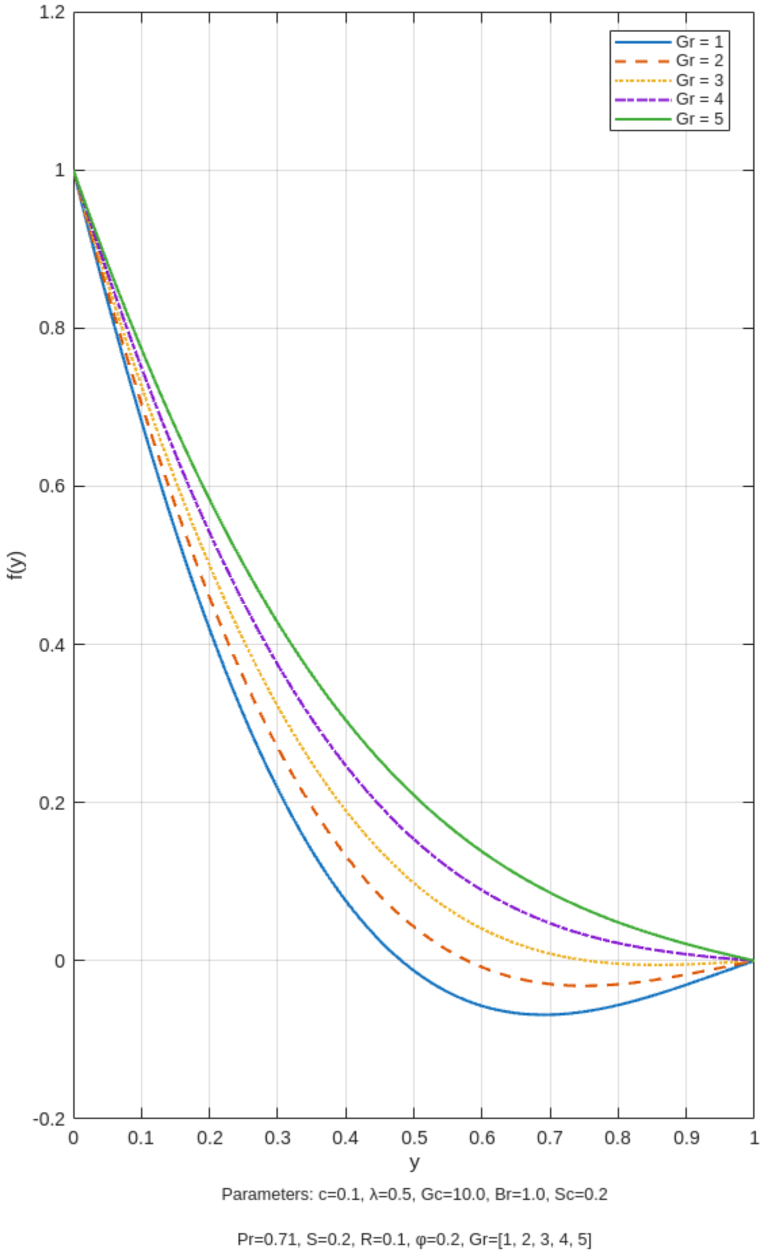

Figure 4.4 Velocity Profile for Various Values of Thermal Grashop number (Gr)

Figure 4.4 described that Increasing Gr leads to stronger buoyancy forces that enhance upward motion, thereby increasing the velocity profile significantly.

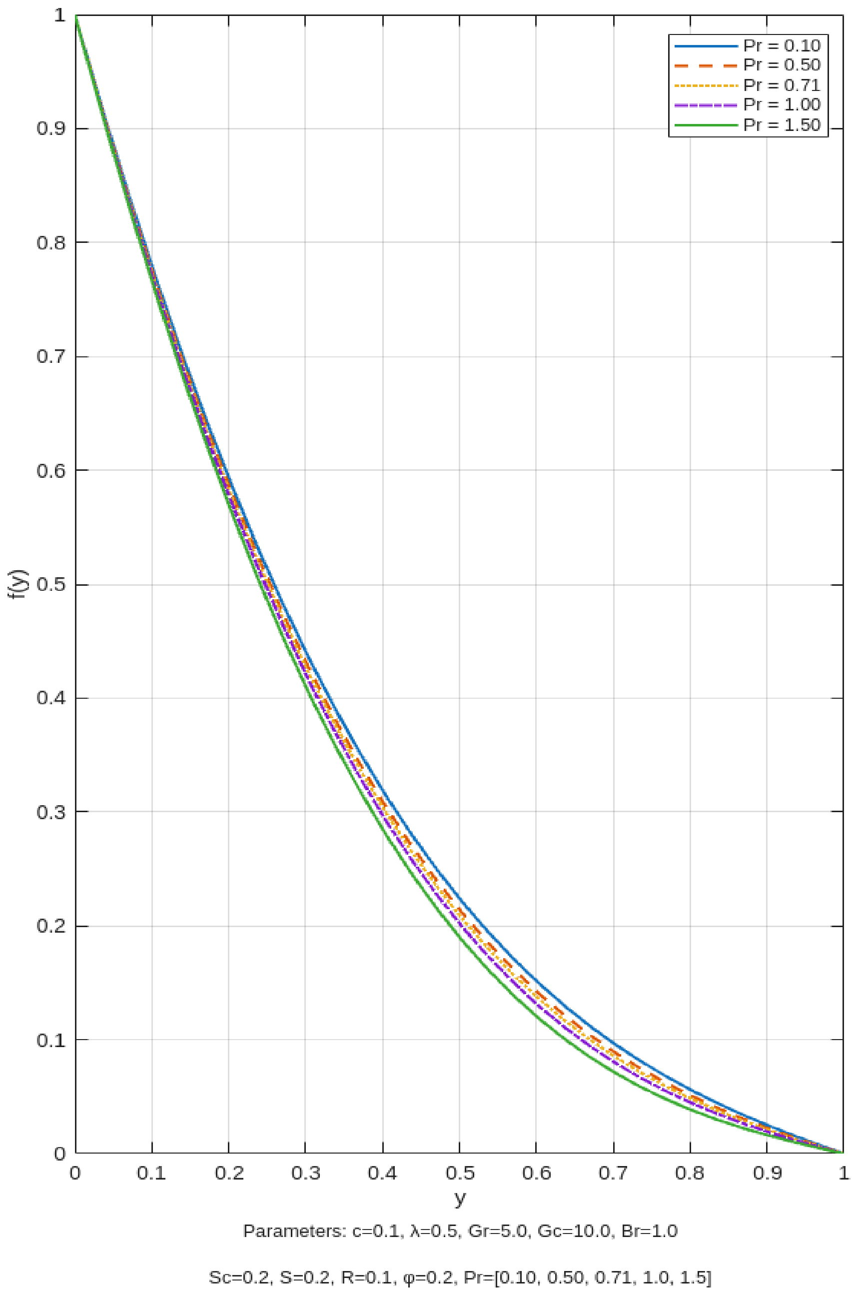

Figure 4.6 Velocity Profile for Various Values of Prandtl Number Parameter (Pr)

In figure 4.6 above Higher Pr reduces velocity due to weaker thermal diffusivity and thinner hydrodynamic boundary layers.

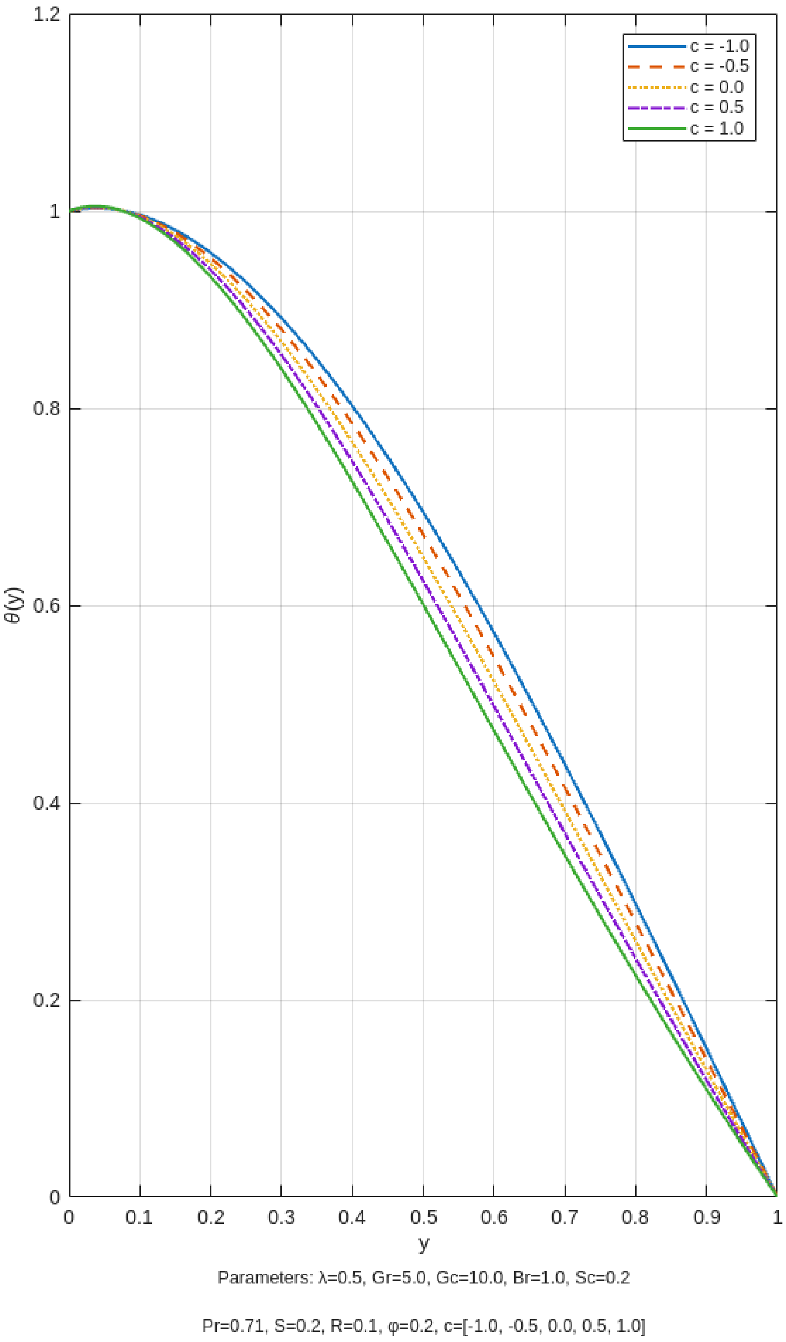

Figure 4.11 Temperature Profile for Various Values of Suction Parameter (C)

The temperature decreases with increasing C from the figure 4.11 above, as suction removes heated fluid and enhances cooling of the system. Conversely, injection leads to thicker thermal layers and higher temperatures.

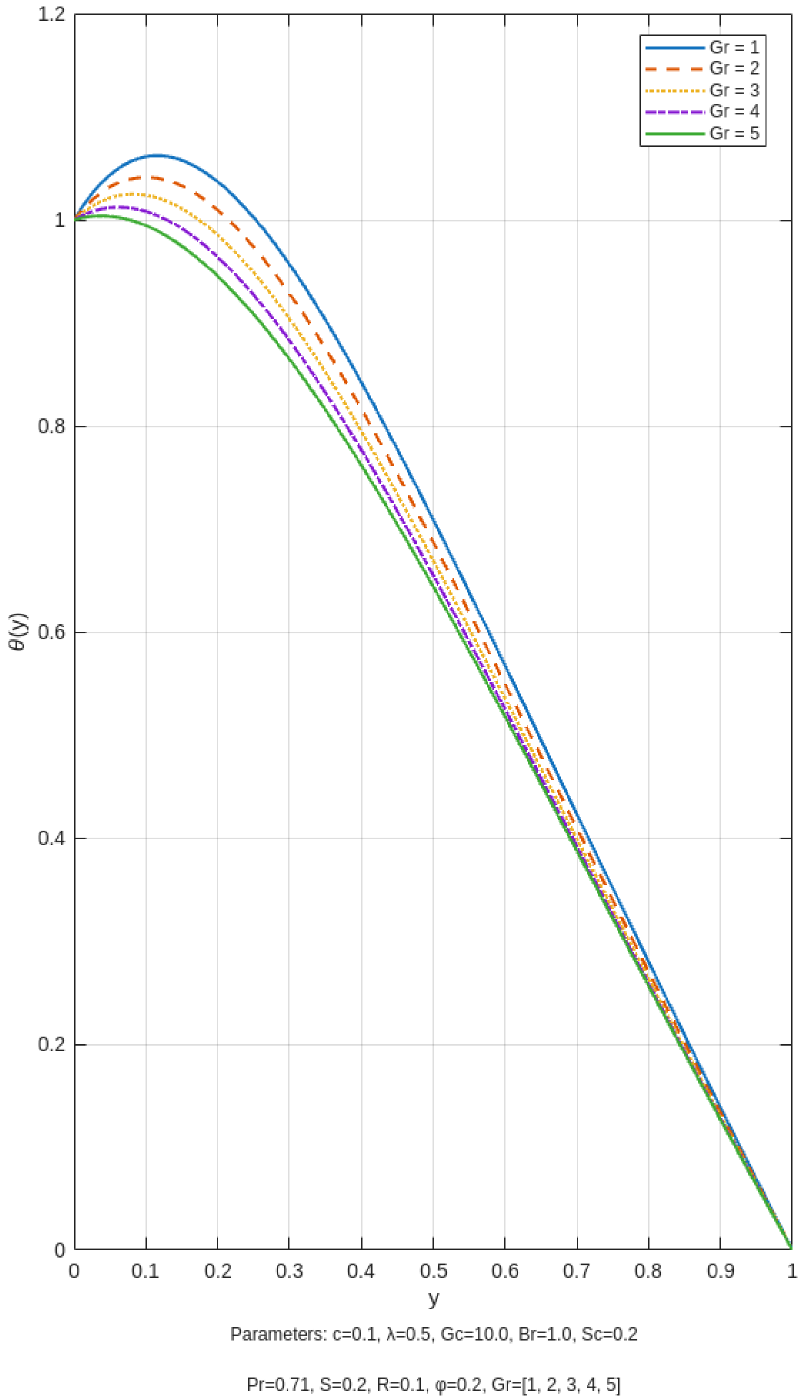

Figure 4.13 Temperature Profile for Various Values of Thermal Grashop Number Parameter (Gr)

Figure 4.13 displayed that, the temperature slightly increases with higher Gr due to stronger thermal convection enhancing heat transfer within the flow.

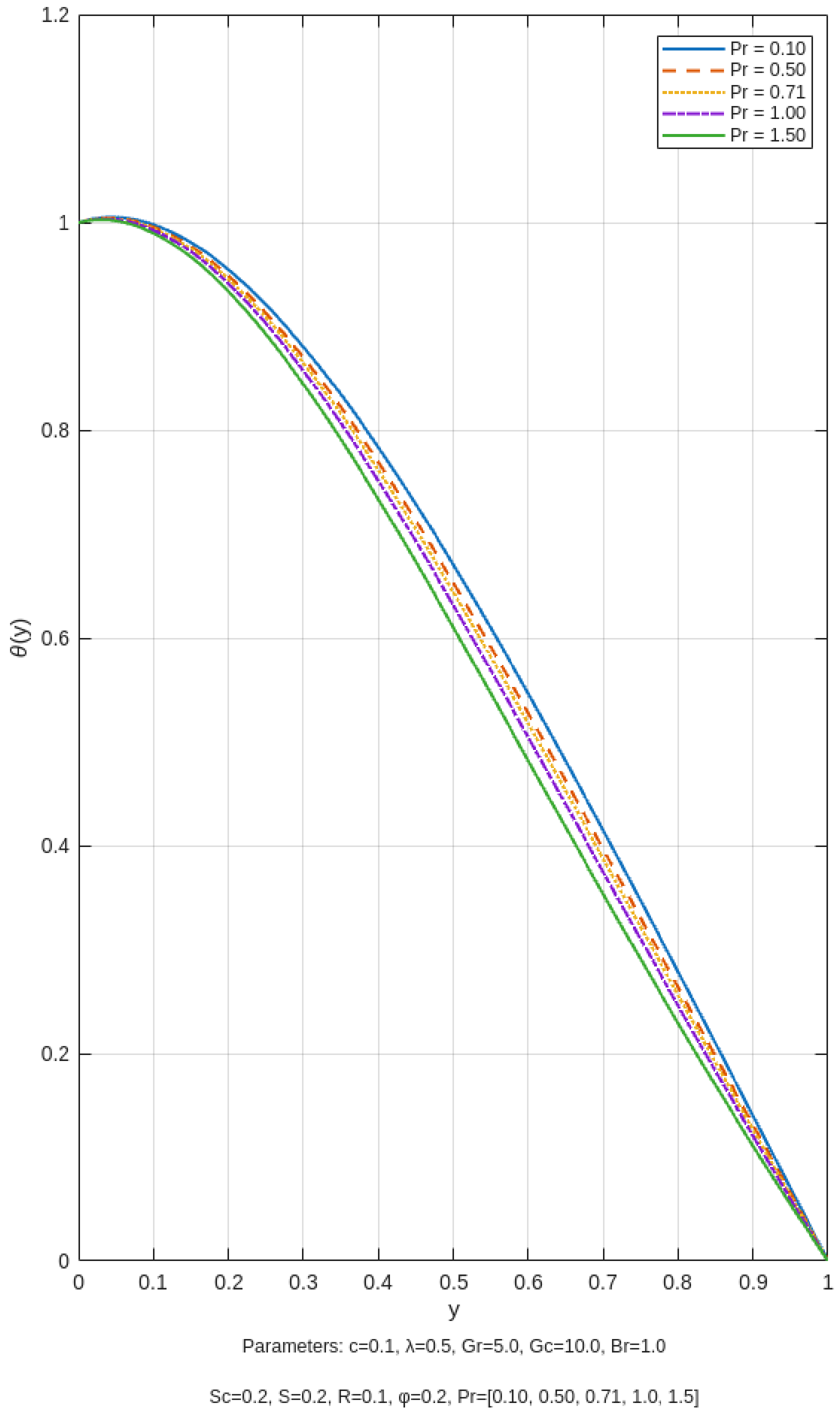

Figure 4.15 Temperature Profile for Various Values of Prandtl Number Parameter (Pr)

It is sighted that, Temperature profile becomes steeper as Pr increases from figure 4.15 above, since fluids with higher Pr retain heat closer to the wall and conduct it less effectively.

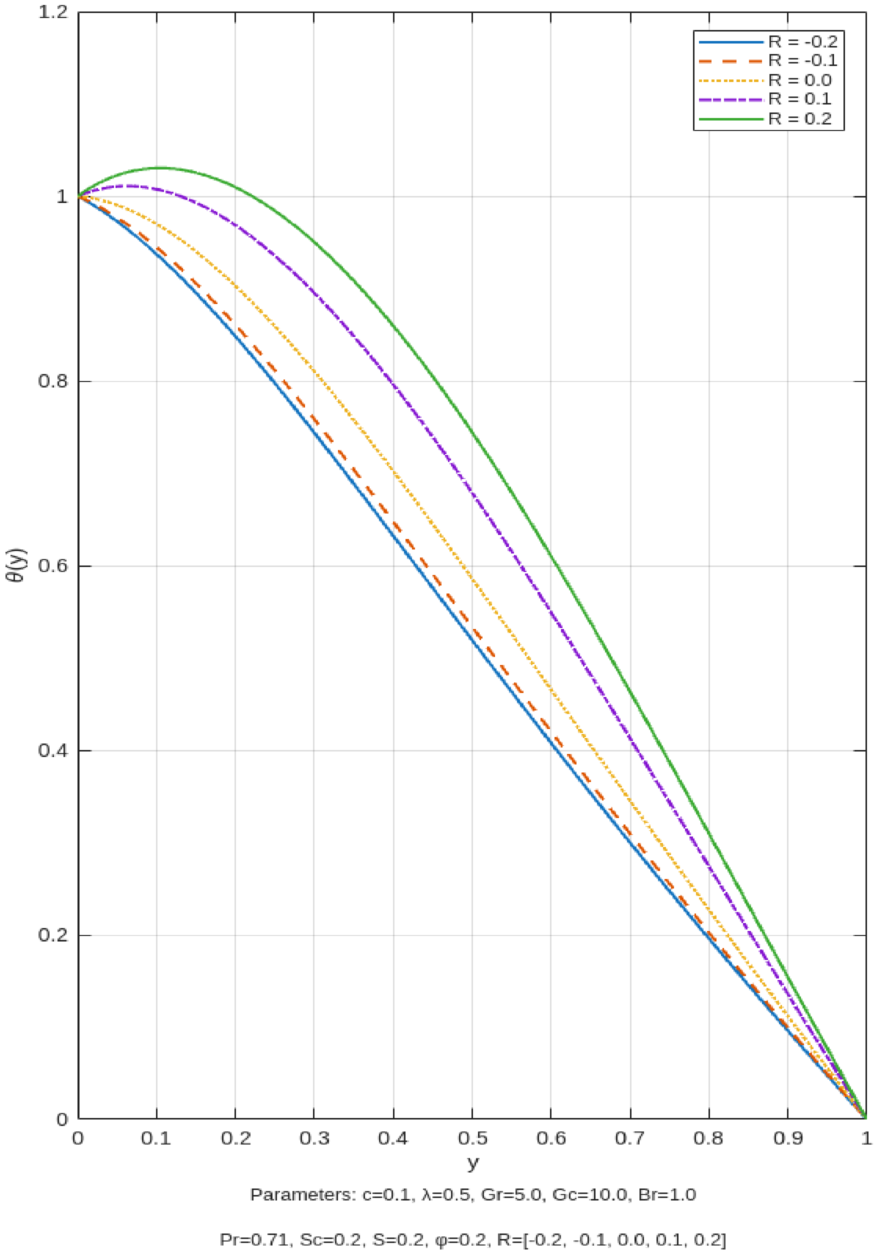

Figure 4.18 Temperature Profile for Various Values of Radiation Parameter (R)

Figure 4.18 described that, the temperature is highly sensitive to R, with negative values enhancing cooling and positive values increasing thermal energy within the flow.

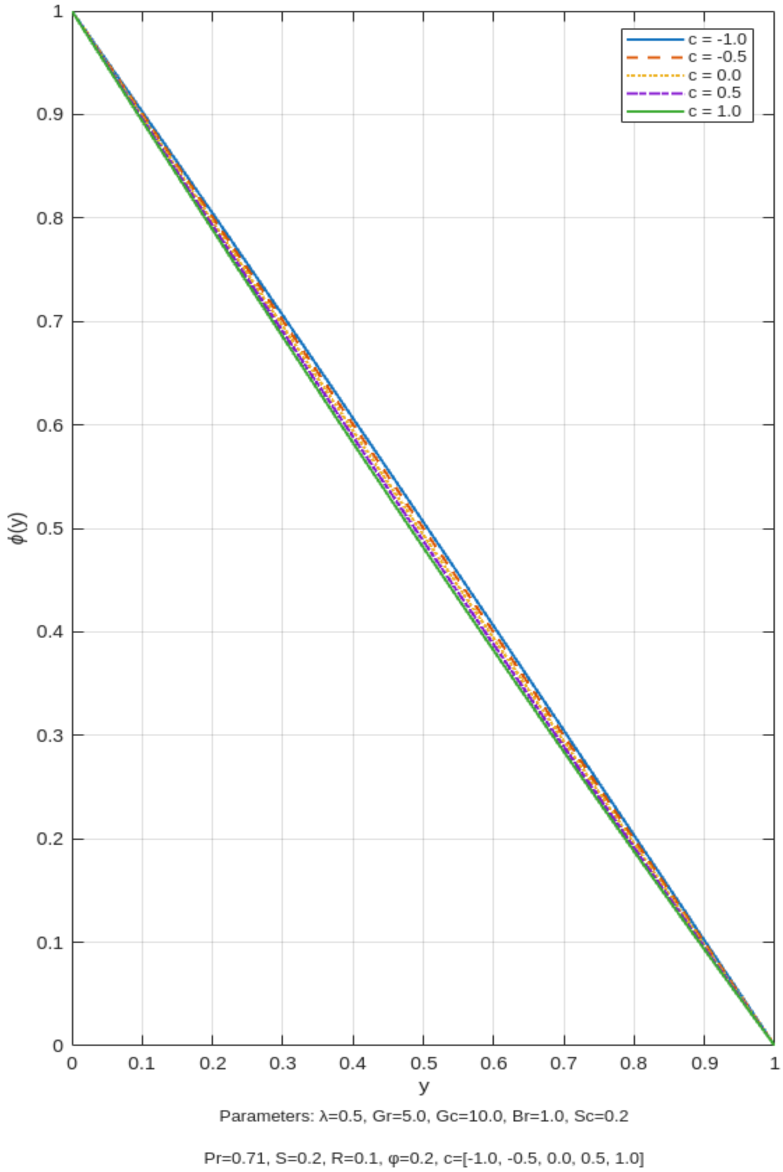

Figure 4.19 Concentration Profile for Various Values of Suction Parameter (C)

Figure 4.19 displayed that, Concentration shows only a slight decrease with increasing C. This means suction has only a minimal effect on species transport, indicating that mass diffusion dominates over suction effects.

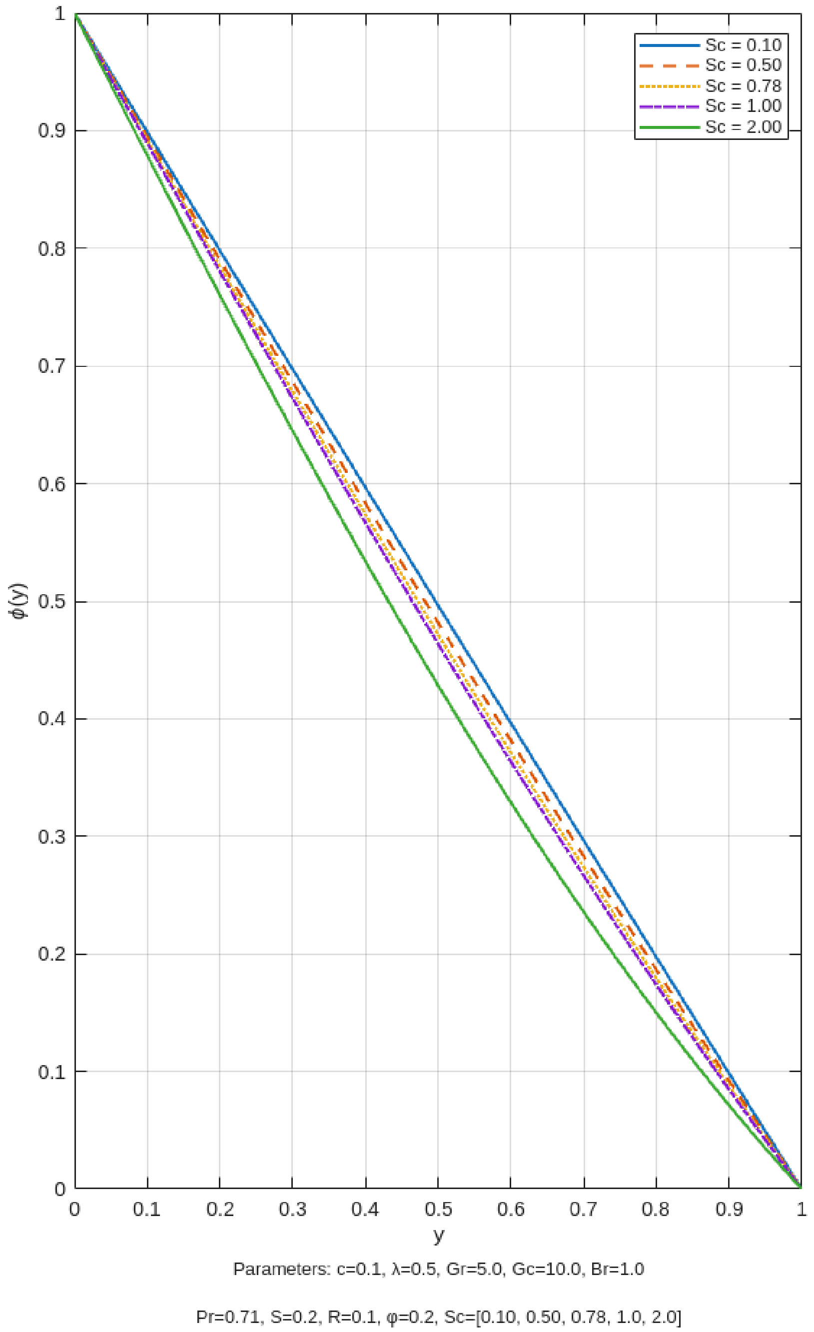

Figure 4.20 Concentration Profile for Various Values of Scmidlt Number Parameter (Sc)

From figure 4.20 above, the concentration gradient becomes sharper near the wall at higher Sc, indicating reduced mass diffusion and thinner concentration boundary layers

© IIJP 2025 | Volume 1, Issue 4, pp. 82-105 | ISSN: 2636-4484

Table 4.2: Numerical Values of Skin Friction on the Walls of Problem 1.

Pr	R = 0.1, ϕ=0.2, Gr = 5, Q = 0.2, C = 0.1, Br = 0.5, Sc=0.2, Gc = 10, Pr = 0.71		R = 0.2, ϕ = 0.2, Gr = 5, Q = 0.2, Gc = 10, Pr = 0.71 C = 0.1, Br = 0.5, Sc=0.2		R=0.1, φ=0.5, Gr=5, Q = 0.2, c=0.1, Br=0.5, Sc=0.2, Gc = 10, Pr = 0.71.	
	τ0	τ1	τ0	τ1	τ0	τ1
0.5	2.41335901002427	0.301325950800579	2.21923651391209	0.402482746751467	2.22800688935886	0.403488666767582
1	2.36330952211047	0.337953099231516	2.16613568706495	0.443369034737974	2.1737647163049	0.445177459851924
1.5	2.31412954043057	0.374316384739107	2.11376602947568	0.484029546639329	2.12039743822944	0.48654437639853
2.0	2.26596138967838	0.410264644118966	2.06228253785852	0.524273823239331	2.06809952921	0.527363583220886
2.5	2.2189323426539	0.445651884948048	2.01186078755906	0.563893412424787	2.01708150793016	0.567393290865305

Table 4.2: The data demonstrates that an increase in the variable viscosity parameter (λ) results in a definitive decrease in skin friction on both channel walls. Furthermore, for fixed values of other parameters, skin friction is also observed to decrease as the radiation parameter (R) and the concentration buoyancy parameter (ϕ) increase.

© IIJP 2025 | Volume 1, Issue 4, pp. 82-105 | ISSN: 2636-4484

Table 4.3: The Numerical Figures for the Heat Transfer Rate on the Channel Walls of Problem 1.

λ	R = 0.1, φ=0.2, Gr = 5, Gc=10 C = 0.1, Br = 0.5, Sc=0.5, Q = 0.2.		R = 0.2, φ = 0.2, Gr = 5, Gc=10, Q = 0.2, C = 0.3, Br = 0.5, Sc=0.2		R=0.3, φ=0.5, Gr=5, Gc=10 c=0.1, Br=0.5, Sc=0.2, Q = 0.2.	
	Nu_0	Nu_1	Nu_0	Nu_1	Nu_0	Nu_1
0.1	0.188143481025527	1.46607956447805	0.129150899729569	1.74281893504578	0.102970154541282	1.77838054509082
0.3	0.202317869874991	1.45599950309708	0.101761384680299	1.72696779083821	0.0768315895659732	1.76257302347711
0.5	0.267983373228253	1.43519405959476	0.00346473746672959	1.68603053078715	0.0179739601736451	1.7231971416733
0.7	0.382072159153624	1.40350471656147	0.152388992067609	1.62389841799736	0.170630578853093	1.6627605156066
0.9	0.539026070094673	1.36200223940928	0.349691198382007	1.54765721722586	0.36728934112833	1.5870845506393

Table 4.3: This table reveals the contrasting effect of the Prandtl number (Pr) on the heat transfer rate (Nusselt number) across the channel walls; an increase in Pr leads to an increase at the wall y=0 but a decrease at y=1. Similarly, an increase in the radiation parameter (R) increases the Nusselt number at y=0 while decreasing it at y=1. The suction parameter (c) also has an asymmetric impact, decreasing the heat transfer rate at y=0 and increasing it at y=1.

© IIJP 2025 | Volume 1, Issue 4, pp. 82-105 | ISSN: 2636-4484

Table 4.4: Numerical Values for the Rate of Mass Transfer (Sherwood Number) Rate on the Channel Walls of Problem 1.

Sc	R = 0.1, φ=0.2, Gr = 5, Gc=10 C = 0.1, Pr = 0.71 Br = 0.5, Sc=0.5, Q = 0.2		R = 0.2, φ = 0.2, Gr = 5, Gc = 10, Pr = 2 C = 0.5, Br = 0.5, Sc = 0.2, Q = 0.2		R = 0.1, φ = 0.5, Gr=5, Gc=10 C=0.1, Br=0.5, Sc=0.2, Pr=0.71, Q = 0.2	
	Sh_0	Sh_1	Sh_0	Sh_1	Sh_0	Sh_1
0.1	0.999395035055051	1.02896076228238	0.999394736292369	1.02896128858577	0.999394781186613	1.02896120949961
0.3	0.978101619084526	1.06750139019635	0.978100726104214	1.06750299202091	0.978100860289888	1.06750275131917
0.5	0.956968416245585	1.10714612414274	0.956966914529733	1.10714886698246	0.956967156323885	1.10714842535258
0.7	0.936002142184589	1.14790839117389	0.936000152605687	1.1479120913473	0.936000514969682	1.14791141743098
0.9	0.915209663332184	1.18980048835824	0.915207273471874	1.18980501413079	0.915207683707608	1.18980423725119

Table 4.4: The results highlight that an increase in the Schmidt number (Sc) causes the mass transfer rate (Sherwood number) to increase at wall y=0 and decrease at wall y=1. The suction parameter (c) shows a similar divergent effect, increasing the Sherwood number at y=0 while decreasing it at y=1. Notably, even the Prandtl number (Pr) influences mass transfer, with an increase leading to a higher Sherwood number at y=0 and a lower one at y=1.

9.0 CONCLUSION

The present numerical investigation examined mass transfer in a vertical channel under the combined influence of temperature-dependent viscosity, thermal radiation, and suction using the finite difference method. The governing equations were implemented in MATLAB and simulated with results displayed graphically and in tables. The analysis revealed that a reduction in the Grashof number leads to a decline in fluid velocity, while an increase in the Prandtl number enhances both velocity and temperature distributions. Similarly, higher values of the radiation parameter were found to augment the velocity field, whereas an increase in the Schmidt number suppresses both velocity and concentration profiles. Collectively, these results provide valuable insight into the coupled effects of viscosity variation, radiation, and suction on convective transport in vertical channels, offering guidance for the analysis and optimization of thermal and mass transfer processes in engineering systems.

10.0 ACKNOWLEDGEMENT

The researchers wish to acknowledge the effort of Dr Auwal Yusuf Bichi of the department of mathematics, Federal University, Dutsin-Ma Katsina State; for his support and guidance. Similarly, the authors acknowledge the efforts of Dr Yusuf Bello of the department of Mathematics and Statistics, Federal University Dutsin-Ma Katsina State Nigeria.

REFERENCES

Ahmed, N., Awais, M., & Arif, M. (2021). Finite element simulation of curved channel MHD convection with thermal radiation. *Alexandria Engineering Journal,* 60(6), 5339–5351.

Alharbi, S. O., Khan, W. A., & Gorla, R. S. R. (2014). Lateral mass flux and thermal radiation effects on natural convection with Soret and Dufour effects in porous media. J*ournal of King Saud University – Engineering Sciences,* 26(2), 161–170.

Bao, J., Li, X., & Zhao, W. (2023). Freeze range in helium-chilled copper tubes following sudden vacuum loss. *International Journal of Heat and Mass Transfer,* 207, 123467.

Das, K., Jana, S., & Kundu, P. K. (2020). MHD free convection flow in a vertical channel with radiation. *Heat Transfer,* 49(8), 5129–5145.

Elgazery, N. S. (2011). Radiation effects on MHD convection in porous media. *Applied Mathematics and Computation,* 217(12), 5362–5374.

Ferdousi, R., Rahman, M. M., & Alam, M. S. (2013). Effects of variable viscosity and radiation on natural convection in a porous medium with internal heat generation. *Nonlinear Analysis: Modelling and Control,* 18(2), 151–163.

Hossain, M. A., & Wilson, M. (2003). Unsteady natural convection flow past an impulsively started vertical plate. *International Journal of Thermal Sciences,* 42(8), 777–783.

Ivanova, M., Petrov, A., & Zhang, Y. (2024). A unified approach for rapid mass transfer in binary systems. *Astrophysical Journal,* 950(1), 35.

Kumar, R., & Singh, P. (2022). Improved numerical schemes for convection–radiation problems in porous media. *Journal of Computational and Applied Mathematics,* 404, 113793.

Li, Z., Chen, Q., & He, Y. (2020). Lattice Boltzmann simulation of unsteady convection with wall roughness. *Physics of Fluids,* 32(12), 123601.

Mahdy, A., & Chamkha, A. J. (2019). Darcy dissipation effects on mixed convection with radiation. *Journal of Porous Media,* 22(5), 455–470.

Makinde, O. D., & Ogulu, A. (2008). Radiation and variable viscosity effects on MHD free convection in a porous medium. *International Communications in Heat and Mass Transfer,* 35(4), 508–513.

Raptis, A., & Perdikis, C. (2006). Thermal radiation effects on viscous flow past a semi-infinite vertical plate. *International Journal of Applied Mechanics and Engineering,* 11(2), 289–297.

Roy, N. C., Debnath, S., & Alam, M. S. (2021). Unsteady MHD free convection in a vertical channel with thermal radiation. *Mathematics and Computers in Simulation,* 185, 82–94.

Wang, B., Xu, J., & Li, H. (2022). Shear flow over staggered herringbone microstructures: Lattice Boltzmann simulations. *International Journal of Heat and Mass Transfer,* 188, 122636.

Zaheer, T., & Tasawar, H. (2007). Radiation effects on boundary layer flow and heat transfer over a vertical plate. *Communications in Nonlinear Science and Numerical Simulation,* 12(6), 791–803.

11.0 NOMENCLATURE

Symbol	Description	Unit
y'	Dimensional length	mm
y	Dimensionless length	–
g	Gravitational acceleration	m/s²
k	Thermal conductivity	W/m·K
T	Dimensional temperature	K
H	Channel width (dimensional)	m
T_w	Wall temperature	K
T_∞	Ambient temperature	K
U'	Dimensional velocity	m/s
U	Dimensionless velocity	–
μ	Dynamic viscosity	kg/m·s
μ_0	Initial fluid viscosity	kg/m·s
ν (mu/ρ)	Kinematic viscosity	m²/s
α	Thermal diffusivity	m²/s
β	Volumetric expansion coefficient	1/K
R	Thermal radiation parameter	–
S	Heat generation/absorption parameter	–
q_r	Radiative heat flux	W/m²
φ	Temperature difference parameter	K
θ	Dimensionless temperature	–
σ	Stefan–Boltzmann constant	W/m²·K⁴
ε	Thermal conductivity variation parameter	–
λ	Viscosity variation parameter	–
v_0	Dimensional suction velocity	m/s